Highly Efficient Electron Transport Obtained by Doping PCBM with Graphdiyne in Planar-Heterojunction Perovskite Solar Cells

Chaoyang Kuang,[†,§] Gang Tang,[†,§] Tonggang Jiu,*[,†] Hui Yang,[‡] Huibiao Liu,[‡] Bairu Li,[†] Weining Luo,[†] Xiaodong Li,[†] Wenjun Zhang,[†] Fushen Lu,[§] Junfeng Fang,*[,†] and Yuliang Li*[,‡]

[†]Institute of New Energy Technology, Ningbo Institute of Material Technology and Engineering (NIMTE), Chinese Academy of Science (CAS), Ningbo, 315201, Peoples Republic of China

[‡]CAS Key Laboratory of Organic Solids, Beijing National Laboratory for Molecular Sciences (BNLMS), Institute of Chemistry, Chinese Academy of Sciences, Beijing 100190, Peoples Republic of China

[§]College of Science, Shantou University, Shantou, 515063, Peoples Republic of China

Supporting Information

ABSTRACT: Organic–inorganic perovskite solar cells have recently emerged at the forefront of photovoltaics research. Here, for the first time, graphdiyne (GD), a novel two dimension carbon material, is doped into PCBM layer of perovskite solar cell with an inverted structure (ITO/PEDOT:PSS/$CH_3NH_3PbI_{3-x}Cl_x$/PCBM:GD/C_{60}/Al) to improve the electron transport. The optimized PCE of 14.8% was achieved. Also, an average power conversion efficiency (PCE) of PCBM:GD-based devices was observed with 28.7% enhancement (13.9% vs 10.8%) compared to that of pure PCBM-based ones. According to scanning electron microscopy, conductive atomic force microscopy, space charge limited current, and photoluminescence quenching measurements, the enhanced current density and fill factor of PCBM:GD-based devices were ascribed to the better coverage on the perovskite layer, improved electrical conductivity, strong electron mobility, and efficient charge extraction. Small hysteresis and stable power output under working condition (14.4%) have also been demonstrated for PCBM:GD based devices. The enhanced device performances indicated the improvement of film conductivity and interfacial coverage based on GD doping which brought the high PCE of the devices and the data repeatability. In this work, GD demonstrates its great potential for applications in photovoltaic field owing to its networks with delocalized π-systems and unique conductivity advantage.

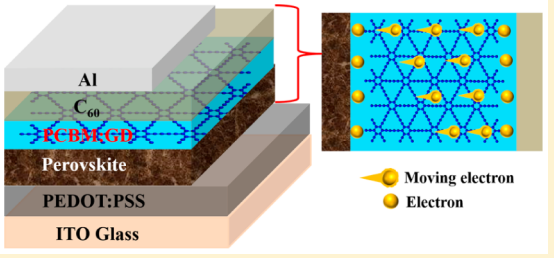

KEYWORDS: *Graphdiyne doping, perovskite solar cell, PCBM, electrical conductivity, interfacial coverage*

Organic–inorganic hybrid perovskite solar cells have attracted intense attention due to their large absorption coefficient, high charge carrier mobility, electron–hole diffusion length, easy fabrication, and low-cost.[1−13] Great success has been attained by elevating the power conversion efficiency (PCE) to over 19% within several years since its birth.[14] Following the absorption of incident photons, carriers are generated within the bulk of perovskite absorber. More importantly efficient charge extraction requires selective contacting of the perovskite layer with a positive (p) and a negative (n) contact material. As we know, diffusion length of the electrons is shorter than that of the holes, which is a major limitation in enhancing PCEs of perovskite solar cells.[15] Yang group achieved the higher PCE of 19.3% by building the interface engineering of electron transport layer (ETL).[16] So it is very important to improve the electrons transport properties in perovskite solar cells. N-type organic molecule such as phenyl-C_{61}-butyric acid methyl ester (PCBM)[17] or metal oxides such as ZnO,[18] TiO_2,[19,20] and so forth are usually employed as the ETLs to achieve the higher efficiencies of perovskite solar cells. Among them, PCBM has already been intensively applied in the P–I–N structure.[21−23] However, there are several problematic issues such as low coverage, leakage currents, interfacial recombination, and so on needed to be resolved, which result in relatively poor photovoltaic performance. Therefore, doping or modification of the PCBM layer ought to be made to achieve higher photocurrents and better coverage for high-performance perovskite solar cells.

Carbon materials,[24−26] such as graphdiyne[27−34] (GD), graphene,[35,36] graphene oxide,[37] and single-walled carbon nanotubes[38,39] (SWNTs), are emerging dopant in perovskite solar cells due to their unique conductivity advantages. Snaith group has applied graphene nanocomposites and carbon nanotube into perovskite solar cells as electron collection layer and obtained high PCE.[38,39] Unlike graphite and graphene, GD possesses both sp- and sp^2-hybridized carbon atoms and natural holes, resulting in many interesting applications such as Li storage, oxygen reactions electronic

Received: February 26, 2015
Revised: March 21, 2015
Published: March 24, 2015

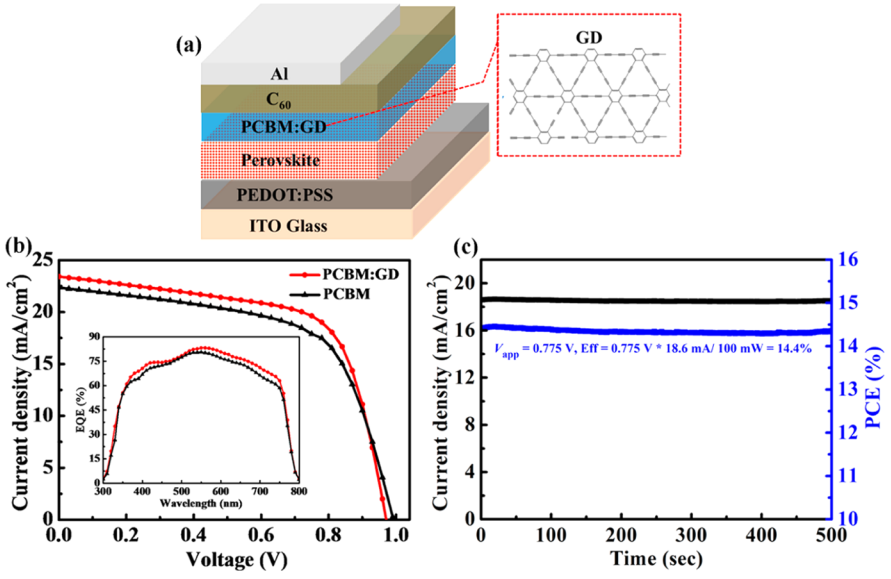

Figure 1. (a) Device architecture of perovskite solar cell and chemical structure of graphdiyne. From the bottom: glass/ITO/PEDOT:PSS/Perovskite/PCBM:GD/C_{60}/Al. (b) $J-V$ characteristic curves of pure PCBM and PCBM:GD based perovskite solar cells under AM 1.5G 100 mW/cm^2 simulated solar light. Inset is corresponding external quantum efficiency (EQE) spectra of the optimal PCBM:GD and PCBM based devices. (c) Steady-state efficiency (blue) with the photocurrent density (black) of the optimal PCBM:GD based perovskite solar cell device as a function of time applied at a forward bias of 0.775 V.

devices, and catalyst.[27−34] Carbon networks of GD with delocalized π-systems are of particular interest owing to the tenability of their properties with clever changes in their electronic, optic, and geometric characteristics.[40] Recently, GD has been introduced into perovskite solar cells as a dopant into poly(3-hexylthiophene) (P3HT) working as hole-transporting material (HTM) for effective hole transport.[41] GD displayed relatively strong $\pi-\pi$ stacking interaction between GD particles and P3HT, but detailed analysis of the increased short circuit current density (J_{sc}) was lacked.

In this work, for the first time we built the electron transport layer composed of PCBM doped with GD in planar heterojunction (PHJ) $CH_3NH_3PbI_{3-x}Cl_x$ solar cells. This introduction of GD led to the improved performance of PHJ perovskite solar cells with the PCE increased from 13.5 to 14.8% and the J_{sc} increased from 22.3 to 23.4 mA/cm^2. It was found that the doping GD not only increased electrical conductivity, electron mobility, and charge extraction ability in the ETL layer but also improved the ETL film coverage on perovskite layer that was very important for the data repeatability. Several measurements such as scanning electron microscopy (SEM), conductive atomic force microscope (c-AFM), the space charge limited current (SCLC), and photoluminescence (PL) were conducted to give detailed analysis of the improved device performances. The results indicated that the introduction of GD dopant into PHJ perovskite solar cells was an effective strategy for enhancing device performance.

Results and Discussion. The device structure of PHJ perovskite solar cells in this study was ITO/PEDOT:PSS/$CH_3NH_3PbI_{3-x}Cl_x$/PCBM:GD/C_{60}/Al, as shown in Figure 1a. The chemical structure of GD is presented on the right. The resultant current density (J)−voltage (V) characteristics based on this device structure under AM 1.5 G conditions (100 mW/cm^2) are displayed in Figure 1b and the relevant parameters were summarized in Table1 (reference devices based on PCBM were also fabricated and measured). The control device based

Table 1. Parameters of Optimized Devices Based on Different Electron Transport Layers[a]

				PCE(%)		
ETL	V_{oc} (V)	J_{sc} (mA/cm^2)	FF (%)	best	average	R_s (Ω cm^2)
Pure PCBM	0.989	22.3	61.5	13.6	10.8	7.5
PCBM:GD	0.969	23.4	65.4	14.8	13.9	5.5

[a]The average values were obtained from eight cells.

on pure PCBM interlayer exhibited a J_{sc} of 22.3 mA/cm^2, an open-circuit voltage (V_{oc}) of 0.989 V, a fill factor (FF) of 0.615 with a corresponding PCE of 13.6% (average PCE of 10.8%). While the device using PCBM:GD as electron transport layer displayed a J_{sc} of 23.4 mA/cm^2, a V_{oc} of 0.969 V and a FF of 0.654, yielding a PCE of 14.8% (average PCE of 13.9%). Corresponding external quantum efficiency (EQE) spectra of this device and the control device were displayed in Figure 1b inset. The spectra showed the same tendency but different height corresponding to conductivity difference from GD doping. The band edge presented the same wavelength at ~775 nm with the absorption edge of perovskite layer, as shown in Figure S1 (Supporting Information). A remarkable higher average PCE of PCBM:GD-based devices was observed with 28% enhancement (13.9% vs 10.8%) compared to that based on pure PCBM-based ones. The V_{oc} values from PCBM:GD-based devices slightly decreased compared to control devices. An approximately 200 mV surface potential decrease (Figure S2 in Supporting Information) in PCBM:GD film compared with that of pure PCBM film was observed, which may explain the declining V_{oc}.[42−44] However, both enhanced J_{sc} and FF were observed from the PCBM:GD-based device. As expected, the enhancement of J_{sc} was obvious due to the high conductivity of GD.

In order to figure out whether the notable over 14% PCE for our device was reliable or not. The stabilized photocurrent output[45−48] of the optimal PCBM:GD based device was

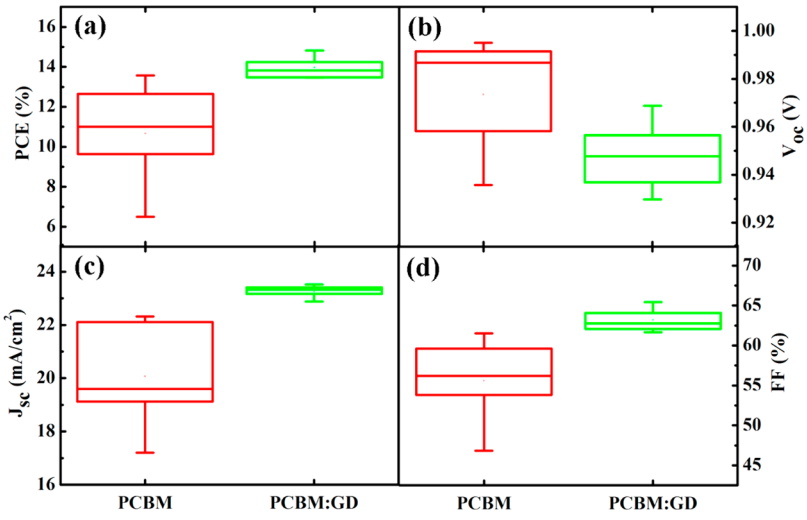

Figure 2. Performance data based on devices with PCBM and PCBM:GD electron transport layers were represented as a standard box plot shown in (a) PCE, (b) V_{oc}, (c) J_{sc}, and (d) FF.

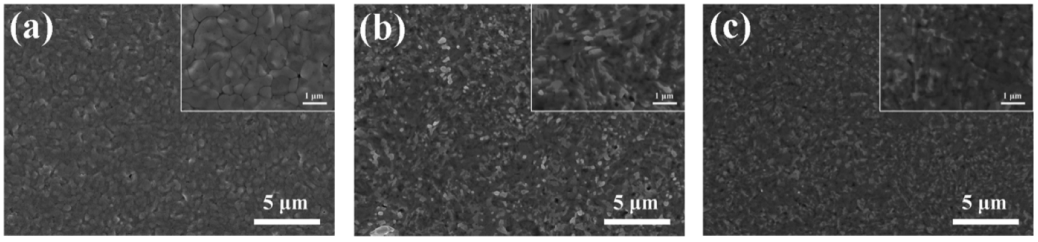

Figure 3. Top view SEM images of (a) ITO/PEDOT:PSS/perovskite thin film, (b) PCBM-coated perovskite layer on ITO/PEDOT:PSS substrate, and (c) PCBM:GD-coated perovskite layer on ITO/PEDOT:PSS substrate. Insets are magnified images for each film and scale bar is 1 μm.

measured held at a forward bias of 0.775 V (voltage of the maximum power point). A steady-state PCE of 14.4% was obtained, as shown in Figure 1d. Only a 2.7% drop in efficiency was observed, which outperformed other cells employing only dense-TiO_2.[48] This result indicated that the optimized PCE in our device was reliable.

Furthermore, in order to exclude the experiment accidental errors, the statistical data of eight devices fabricated with pure PCBM and PCBM:GD electron transport layers were presented in the form of a standard box plot,[39,41,49] respectively, as shown in Figure 2. This box plot has been widely used in perovskite solar cells for analyzing the statistical distributions of device parameters. As can be seen, the average V_{oc} of PCBM:GD based devices was lower than that of control devices. The average J_{sc} and FF of PCBM:GD based devices were higher than those of the pure PCBM-based ones. Moreover, the smaller standard deviation of device parameters for the PCBM:GD-based devices as compared with the control devices indicated a higher degree of reproducibility of the best performance devices, especially in the J_{sc}. This results were in well agreement with the above ones.

As we all know, the morphology of perovskite layer and interlayer played an important role in achieving high performance of PHJ perovskite solar cells.[50,51] So SEM measurements were performed, as shown in Figure 3. The perovskite layer in our devices exhibited larger grain and more compact morphology, which brought the favorable device performance in this study. After the perovskite layer was coated with the PCBM or PCBM:GD layer, the surfaces morphologies displayed slightly differences as shown in Figure 3b,c. The rough perovskite layer became smoother when coated by PCBM:GD film than that coated by pure PCBM film. The graphdiyne may also help to passivate the grain-boundary of the perovskite and then reduce the trap states of the surface to eliminate the recombination.[21] The improved morphology ensured efficient coverage of ETL together with smaller R_s (5.5 vs 7.5 Ω cm^2), explaining the improved FF in PCBM:GD-based devices.

To characterize the influence of GD-doping on the electronic property of PCBM film and figure out the origin of J_{sc} increment, the conductivity of pure PCBM film and PCBM:GD film was examined by performing c-AFM measurements[52,53] as described in Figure 4a,b. The c-AFM images of PCBM:GD film clearly showed different current levels and distributions from pure PCBM film. Significantly increased vertical current was observed in the PCBM:GD film. The result suggested the electrical conductivity of PCBM:GD increased upon GD-doping. This explained the J_{sc} increment in some ways. However, this is not enough that the higher electrical conductivity of PCBM:GD films brought the higher J_{sc} when used in perovskite devices. To further explore the origins of the enhanced J_{sc}, the electron mobility was approximated using space charge limited current measurements[54] in which device structures were ITO/ZnO/PCBM or PCBM:GD/Ca/Al. Then $J-V$ characteristics of single-carrier devices were measured. The results were plotted as $\ln(JL^3/V^2)$ versus $(V/L)^{0.5}$ by fitting to the Mott–Gurney law, as shown in Figure 4c. Electron mobility was calculated from the intercept of the corresponding lines on the axis of $\ln(JL^3/V^2)$. It is easy to obtain that electron mobility of pure PCBM based electron-only device was 2.98 × 10^{-4}

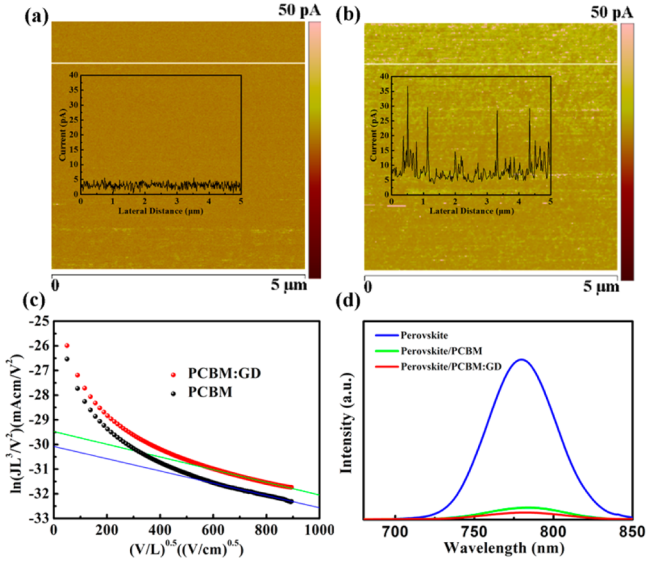

Figure 4. Conductive AFM images of (a) ITO/PCBM and (B) ITO/PCBM:GD film with a scan size of 5 × 5 μm^2. (c) Current−voltage data from the devices of ITO/ZnO/PCBM or PCBM:GD/Ca/Al, plotted in the format $\ln(JL^3/V^2)$ versus $(V/L)^{0.5}$, where J is the current density and L is the thickness of the PCBM or PCBM:GD layer. The lines are the fit to the respective experimental points. (d) The PL spectra of various thin films.

$cm^2/(V\ s)$. After GD doping, the electron mobility of PCBM:GD based electron-only device increased to 5.32×10^{-4} $cm^2/(V\ s)$. The result exhibited that the charge transport mobility of PCBM film was increased by GD doping.

In order to investigate if PCBM:GD film efficiently extract photogenerated carriers from the perovskite absorber, PL spectra were measured as well, as shown in Figure 4d.[15,52] In our devices, PEDOT:PSS, as hole transport layer, and PCBM:GD, as electron transport layer, can extract photogenerated carriers. The PL of PEDOT:PSS/$CH_3NH_3PbI_{3-x}Cl_x$, PEDOT:PSS/$CH_3NH_3PbI_{3-x}Cl_x$/PCBM, and PEDOT:PSS/$CH_3NH_3PbI_{3-x}Cl_x$/PCBM:GD on glass substrates was measured. The excitation light entered the sample from the glass substrate side with excitation at 600 nm, and PL spectra were collected. We observed a significant quenching effect when the perovskite layer was coated with either the PCBM:GD layer or the PCBM layer. The PL of PCBM:GD-coated perovskite film was almost completely quenched. It indicated that PCBM:GD film extracted electron more efficiently, which may decrease charge recombination in devices. The result, as shown in Figure 3a−d, demonstrated that doping GD into PCBM can increase electrical conductivity, electron mobility, and charge extraction ability in the ETL layer. Therefore, the enhanced J_{sc} was attributed to all combined effect of these factors.

Recently, unexpected photocurrent hysteresis has been observed in the $J-V$ curves of perovskite solar cells, especially in the planar structure perovskite solar cells.[15,55−57] Therefore, the $J-V$ curves of the devices with different scanning directions were recorded, as shown in Figure 5a,b. The PCE values obtained from the forward bias scan (forward bias to short circuit, FB-to-SC) and the reverse bias scan (short circuit to forward bias, SC-to-FB) of PCBM:GD based device were 14.8% and 13.9%, respectively. Those of the PCBM-based device were 13.6% and 12.0%, respectively. The difference of PCE values between forward bias scans and the reverse bias scan in PCBM:GD based devices is less than that of PCBM-based ones (0.9% vs 1.6%). In addition, the $J-V$ curves of PCBM:GD based devices at different scanning rates with delay time ranging from 50, 100, to 200 ms were also checked, as shown in Figure 5c,d. The $J-V$ curves of PCBM:GD based devices at different scanning rates almost overlapped with each

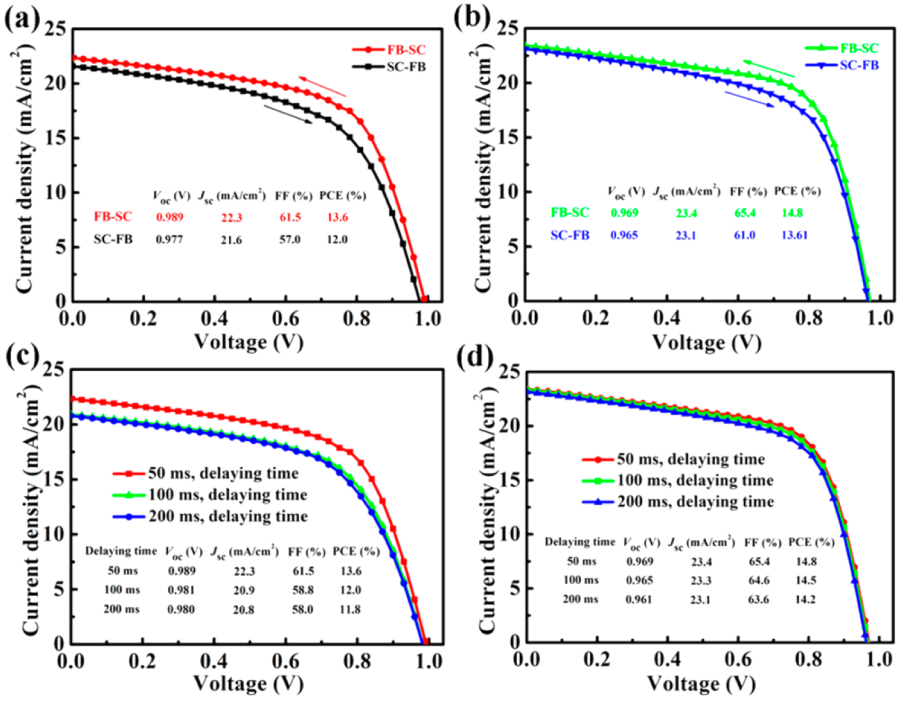

	V_{oc} (V)	J_{sc} (mA/cm²)	FF (%)	PCE (%)
FB-SC	0.989	22.3	61.5	13.6
SC-FB	0.977	21.6	57.0	12.0

	V_{oc} (V)	J_{sc} (mA/cm²)	FF (%)	PCE (%)
FB-SC	0.969	23.4	65.4	14.8
SC-FB	0.965	23.1	61.0	13.61

Delaying time	V_{oc} (V)	J_{sc} (mA/cm²)	FF (%)	PCE (%)
50 ms	0.989	22.3	61.5	13.6
100 ms	0.981	20.9	58.8	12.0
200 ms	0.980	20.8	58.0	11.8

Delaying time	V_{oc} (V)	J_{sc} (mA/cm²)	FF (%)	PCE (%)
50 ms	0.969	23.4	65.4	14.8
100 ms	0.965	23.3	64.6	14.5
200 ms	0.961	23.1	63.6	14.2

Figure 5. $J-V$ characteristic curves of devices with PCBM (a) and PCBM:GD (b) obtained from forward bias to short circuit (FB-SC) and from short circuit to forward bias (SC-FB). $J-V$ characteristic curves of devices with PCBM (c) and PCBM:GD (d) obtained at forward scan direction and different scanning rate with delaying time ranging from 50, 100, to 200 ms.

other while the pure PCBM-based devices showed a large difference at different scanning rates. These results indicated that the photocurrent hysteresis could be reduced to a certain extent by introducing GD in PCBM layer. The weaker photocurrent hysteresis in PCBM:GD based devices may be ascribed to the efficient coverage on perovskite layer and the improved electrical properties.

Conclusion. In conclusion, GD used as a dopant into PCBM ETL layer was successfully applied in PHJ $CH_3NH_3PbI_{3-x}Cl_x$ solar cells for the first time. High efficiency of 14.8%, stable power output (PCE = 14.4%), and small hysteresis PHJ perovskite solar cells based on PCBM:GD ETL were demonstrated. The enhanced J_{sc} and FF were observed from the PCBM:GD based devices. SEM measurement exhibited that the PCBM:GD based devices had better coverage on the rough perovskite layer, which indicated better interfacial contact and less charge recombination. C-AFM, SCLC, and PL measurements further indicated that the introduction of GD into PCBM film could improve the electrical conductivity, electron mobility, and charge extraction. All these results explained the origin of enhanced J_{sc} and FF. So the introduction of carbon materials such as GD into perovskite solar cell applications will become a simple and effective strategy for improving device performances in the future.

Materials and Methods. *Materials.* Poly(3,4-ethylenedioxythiophene):polystyrenesulfonate (PEDOT:PSS) and [6,6]-phenyl-C_{61}-butyric acid methyl ester ($PC_{61}BM$) were purchased from Clevious and American Dye Source Inc., respectively, and used as received without further purification. Lead(II) chloride ($PbCl_2$) and anhydrous *N*,*N*-dimethylformamide (DMF) were purchased from Sigma-Aldrich and used as received without further purification. Methylamine iodide (MAI) was synthesized according to a literature procedure with slight modification.[58] Twenty milliliters of hydroiodic acid (HI), 57 wt % in water (Aladdin) was dropwise added to 48 mL of methylamine, 33 wt % in ethanol (Sigma-Aldrich) in a 250 mL round-bottom flask at 0 °C. This reaction was kept for 2 h with stirring. The precipitate was obtained by putting the solution on a rotary evaporator and carefully removing the solvents at 55 °C. Then, the raw product CH_3NH_3I was redissolved in absolute ethanol and precipitated with diethyl ether. After filtration, the precipitate was washed three times with diethyl ether. A white-colored powder was collected and dried at 60 °C in a vacuum oven for 24 h and used without further purification.

Graphdiyne was synthesized on the surface of copper via a cross-coupling reaction using hexaethynylbenzene. In brief, the monomer of hexaethynylbenzene was synthesized in good yield (62%) by addition of tetrabutylammonium fluoride to tetrahydrofuran solution of hexakis[(trimethylsilyl)ethynyl]-benzene for 10 min at 8 °C. The graphdiyne was successfully grown on the surface of copper foil in the presence of pyridine by a cross-coupling reaction of the monomer of hexaethynylbenzene for 72 h at 60 °C under nitrogen atmosphere.[27,40]

$PC_{61}BM$ solution was prepared by dissolving [6,6]-phenyl-C_{61}-butyric acid methyl ester into chlorobenzene (CB, Aldrich) with a concentration of 20 mg/mL and stirred at 60 °C overnight in glovebox. The GD solution was prepared by dispersing 1.5 mg of GD powder in CB and sonicated at 50 °C for more than 10 h. The $PC_{61}BM$:GD solution was prepared by mixing 500 μL of $PC_{61}BM$ solution (20 mg/mL) with 50 μL of GD solution (1.5 mg/mL).

Perovskite Precursor Preparation. To form the $CH_3NH_3PbI_{3-x}Cl_x$ precursor solution, MAI and $PbCl_2$ (molar ratio 3:1) are dissolved in DMF with final concentrations 2.64 M MAI and 0.88 M $PbCl_2$. This solution was stirred at 60 °C overnight in a N_2-filled glovebox. Prior to device fabrication, the precursor solution was filtered twice with a 0.45 μm PTFE filter.

Device Fabrication. The perovskite solar cells were fabricated on indium tin oxide (ITO)-coated glass substrates (Shenzhen NanBo Group, China, 10Ω/sq) with the following device configuration: ITO/PEDOT:PSS/$CH_3NH_3PbI_{3-x}Cl_x$/$PC_{61}BM$ or $PC_{61}BM$:GD/C_{60}/Al. The ITO-coated glass substrates were cleaned by sequential ultrasonic treatment in detergent, deionized water, acetone, and isopropyl alcohol for 30 min each and then dried with a nitrogen stream. Then the precleaned ITO glasses were moved into an ultraviolet (UV) chamber for UV−ozone treatment for 20 min. A 35 nm thick PEDOT:PSS was spin-coated onto ITO at 4000 rpm for 60 s and then dried at 140 °C for 10 min in air. All substrates were transferred to the glovebox for further processing. Perovskite precursor solution was spin-coated on the PEDOT:PSS layer at 2000 rpm for 45 s. After spin-coating, the films were left to dry at room temperature for 30 min to allow slow solvent evaporation. They were then annealed on a hot plate in the glovebox at 80 °C for 120 min to promote crystallization of the $CH_3NH_3PbI_{3-x}Cl_x$ perovskite and gave the thickness of ∼500 nm. The $PC_{61}BM$ or $PC_{61}BM$:GD layer was then spin-coated onto the $CH_3NH_3PbI_{3-x}Cl_x$ layer at 2000 rpm for 60 s. Finally a 50 nm thick C_{60} and a 100 nm thick aluminum cathode (deposition rate of 1.0 Å/s)) were deposited on the substrates through a shadow mask to give a device area of 0.06 cm^2 under a vacuum level of 10^{-6} Torr. All device measurements were performed in an inert environment.

Device Characterization. The illuminated current density−voltage (*J*−*V*) characteristics of the photovoltaic devices were recorded under illumination and dark conditions using a computer-controlled Keithley 2400 source meter under AM 1.5G simulated solar light. The external quantum efficiency measurements were performed with the Newport IQE-200 Measurement System, which equipped a Xe lamp, a monochromator, a current−voltage preamplifier, and a lock-in amplifier. SEM imaging was conducted on S-4800 scanning electron microscope operated at an acceleration voltage of 8 kV. c-AFM imaging was obtained at room temperature in contact mode by using a Veeco dimension V atomic microscope and the cantilever coated with Pt/Ir while applying a 5 V bias. PL spectra were measured at room temperature by using a fluorescent spectrophotometer (F-4600, Hitachi Ltd., Tokyo, Japan) with a 150W Xe lamp as an excitation source at room temperature.

■ ASSOCIATED CONTENT

Ⓢ Supporting Information

Absorption spectrum of perovskite film and surface potential images of ITO/(PCBM or PCBM:GD) films. This material is available free of charge via the Internet at http://pubs.acs.org.

■ AUTHOR INFORMATION

Corresponding Authors

*E-mail: jiutonggang@nimte.ac.cn (T.J).
*E-mail: fangjf@nimte.ac.cn (J.F.).
*E-mail: ylli@iccas.ac.cn (Y.L.).

Author Contributions

C.K. and G.T. contributed equally to this work.

Notes

The authors declare no competing financial interest.

■ ACKNOWLEDGMENTS

The authors gratefully acknowledge the support of the National Natural Science Foundation of China (Nos. 51202264 and 61474125), and Zhejiang Provincial Natural Science Foundation of China (LR14E030002). The work was also supported by Hundred Talent Program of Chinese Academy of Sciences and Ningbo City Natural Science Foundation of China (2014A610037).

■ REFERENCES

(1) Nie, W.; Tsai, H.; Asadpour, R.; Blancon, J.-C.; Neukirch, A. J.; Gupta, G.; Crochet, J. J.; Chhowalla, M.; Tretiak, S.; Alam, M. A.; et al. *Science* **2015**, *347*, 522−525.
(2) Dong, Q.; Fang, Y.; Shao, Y.; Mulligan, P.; Qiu, J.; Cao, L.; Huang, J. *Science* **2015**, DOI: 10.1126/science.aaa5760.
(3) Liu, L.; Mei, A.; Liu, T.; Jiang, P.; Sheng, Y.; Zhang, L.; Han, H. *J. Am. Chem. Soc.* **2015**, *137*, 1790−1793.
(4) Liu, D.; Yang, J.; Kelly, T. L. *J. Am. Chem. Soc.* **2014**, *136*, 17116−17122.
(5) Xiao, J.; Yang, Y.; Xu, X.; Shi, J.; Zhu, L.; Lv, S.; Wu, H.; Luo, Y.; Li, D.; Meng, Q. *J. Mater. Chem. A* **2015**, DOI: 10.1039/C4TA06700B.
(6) Zhao, D.; Sexton, M.; Park, H.-Y.; Baure, G.; Nino, J. C.; So, F. *Adv. Energy Mater.* **2015**, DOI: 10.1002/aenm.201401855.
(7) Filip, M. R.; Eperon, G. E.; Snaith, H. J.; Giustino, F. *Nat. Commun.* **2014**, *5*, 5757.
(8) Lin, Q.; Armin, A.; Nagiri, R. C. R.; Burn, P. L.; Meredith, P. *Nat. Photonics* **2014**, *9*, 106−112.
(9) Noel, N. K.; Abate, A.; Stranks, S. D.; Parrott, E. S.; Burlakov, V. M.; Goriely, A.; Snaith, H. J. *ACS Nano* **2014**, *8*, 9815−9821.
(10) Xie, F. X.; Zhang, D.; Su, H.; Ren, X.; Wong, K. S.; Gratzel, M.; Choy, W. C. H. *ACS Nano* **2015**, *9*, 639−646.
(11) Liu, M.; Johnston, M. B.; Snaith, H. J. *Nature* **2013**, *501*, 395−398.
(12) You, J.; Hong, Z.; Yang, Y.; Chen, Q.; Cai, M.; Song, T.-B.; Chen, C.-C.; Lu, S.; Liu, Y.; Zhou, H.; Yang, Y. *ACS Nano* **2014**, *8*, 1674−1680.
(13) Chen, Q.; Zhou, H.; Hong, Z.; Luo, S.; Duan, H.-S.; Wang, H.-H.; Liu, Y.; Li, G.; Yang, Y. *J. Am. Chem. Soc.* **2014**, *136*, 622−625.
(14) Jeon, N. J.; Noh, J. H.; Yang, W. S.; Kim, Y. C.; Ryu, S.; Seo, J.; Seok, S., II *Nature* **2015**, *517*, 476−480.
(15) Wang, K.; Liu, C.; Du, P.; Zheng, J.; Gong, X. *Energy Environ. Sci.* **2015**, DOI: 10.1039/C5EE00222B.
(16) Zhou, H.; Chen, Q.; Li, G.; Luo, S.; Song, T.-B.; Duan, H.-S.; Hong, Z.; You, J.; Liu, Y.; Yang, Y. *Science* **2014**, *345*, 542−546.
(17) Wang, Q.; Shao, Y.; Dong, Q.; Xiao, Z.; Yuan, Y.; Huang, J. *Energy Environ. Sci.* **2014**, *7*, 2359−2365.
(18) Zuo, L.; Gu, Z.; Ye, T.; Fu, W.; Wu, G.; Li, H.; Chen, H. *J. Am. Chem. Soc.* **2015**, DOI: 10.1021/ja512518r.
(19) Ryu, S.; Noh, J. H.; Jeon, N. J.; Kim, Y. C.; Yang, W. S.; Seo, J.; Seok, S., II *Energy Environ. Sci.* **2014**, *7*, 2614−2618.
(20) Jeon, N. J.; Lee, H. G.; Kim, Y. C.; Seo, J.; Noh, J. H.; Lee, J.; Seok, S., II *J. Am. Chem. Soc.* **2014**, *136*, 7837−7840.
(21) Shao, Y.; Xiao, Z.; Bi, C.; Yuan, Y.; Huang, J. *Nat. Commun.* **2014**, *5*, 5784.
(22) Bai, Y.; Yu, H.; Zhu, Z.; Jiang, K.; Zhang, T.; Zhao, N.; Yang, S.; Yan, H. *J. Mater. Chem. A* **2015**, DOI: 10.1039/C4TA05309E.
(23) Seo, J.; Park, S.; Kim, Y. C.; Jeon, N. J.; Noh, J. H.; Yoon, S. C.; Seok, S., II *Energy Environ. Sci.* **2014**, *7*, 2642−2646.
(24) Batmunkh, M.; Shearer, C. J.; Biggs, M. J.; Shapter, J. G. *J. Mater. Chem. C* **2015**, DOI: 10.1039/C5TA00873E.
(25) Qian, X.; Liu, H.; Li, Y. *Chin. Sci. Bull.* **2013**, *58*, 2686−2697.
(26) Qian, X.; Liu, H.; Huang, C.; Chen, S.; Zhang, L.; Li, Y.; Wang, J.; Li, Y. *Sci. Rep.* **2015**, *5*, 7756.
(27) Li, G.; Li, Y.; Liu, H.; Guo, Y.; Li, Y.; Zhu, D. *Chem. Commun.* **2010**, *46*, 3256−3258.
(28) Li, G.; Li, Y.; Qian, X.; Liu, H.; Lin, H.; Chen, N.; Li, Y. *J. Phys. Chem. C* **2011**, *115*, 2611−2615.
(29) Liu, R.; Liu, H.; Li, Y.; Yi, Y.; Shang, X.; Zhang, S.; Yu, X.; Zhang, S.; Cao, H.; Zhang, G. *Nanoscale* **2014**, *6*, 11336−11343.
(30) Huang, C.; Zhang, S.; Liu, H.; Li, Y.; Cui, G.; Li, Y. *Nano Energy* **2015**, *11*, 481−489.
(31) Zhang, S.; Liu, H.; Huang, C.; Cui, G.; Li, Y. *Chem. Commun.* **2015**, *51*, 1834−1837.
(32) Wang, S.; Yi, L.; Halpert, J. E.; Lai, X.; Liu, Y.; Cao, H.; Yu, R.; Wang, D.; Li, Y. *Small* **2012**, *8*, 265−271.
(33) Luo, G. F.; Qian, X.; Liu, H.; Qin, R.; Zhou, J.; Li, L.; Gao, Z.; Wang, E.; Mei, W.-N.; Lu, J.; Li, Y.; Nagase, S. *Phys. Rev. B* **2011**, *84*, 075439.
(34) Long, M. Q.; Tang, L.; Wang, D.; Li, Y. L.; Shuai, Z. G. *ACS Nano* **2011**, *5*, 2593−2600.
(35) Wang, J. T.-W.; Ball, J. M.; Barea, E. M.; Abate, A.; Alexander-Webber, J. A.; Huang, J.; Saliba, M.; Mora-Sero, I.; Bisquert, J.; Snaith, H. J. *Nano Lett.* **2014**, *14*, 724−730.
(36) Yang, N.; Liu, Y.; Wen, H.; Tang, Z.; Zhao, H.; Li, Y.; Wang, D. *ACS Nano* **2013**, *7*, 1504−1512.
(37) Zhang, X.; Zhu, M.; Chen, P.; Li, Y.; Liu, H.; Li, Y.; Liu, M. *Phys. Chem. Chem. Phys.* **2015**, *17*, 1217−1225.
(38) Habisreutinger, S. N.; Leijtens, T.; Eperon, G. E.; Stranks, S. D.; Nicholas, R. J.; Snaith, H. J. *J. Phys. Chem. Lett.* **2014**, *5*, 4207−4212.
(39) Habisreutinger, S. N.; Leijtens, T.; Eperon, G. E.; Stranks, S. D.; Nicholas, R. J.; Snaith, H. J. *Nano Lett.* **2014**, *14*, 5561−5568.
(40) Li, Y.; Xu, L.; Liu, H.; Li, Y. *Chem. Soc. Rev.* **2014**, *43*, 2572−2586.
(41) Xiao, J.; Shi, J.; Liu, H.; Xu, Y.; Lv, S.; Luo, Y.; Li, D.; Meng, Q.; Li, Y. *Adv. Energy Mater.* **2015**, DOI: 10.1002/aenm.201401943.
(42) He, Z.; Zhong, C.; Huang, X.; Wong, W.-Y.; Wu, H.; Chen, L.; Su, S.; Cao, Y. *Adv. Mater.* **2011**, *23*, 4636−4643.
(43) Zhou, H.; Zhang, Y.; Seifter, J.; Collins, S. D.; Luo, C.; Bazan, G. C.; Nguyen, T.-Q.; Heeger, A. J. *Adv. Mater.* **2013**, *25*, 1646−1652.
(44) Guo, X.; Zhang, M.; Ma, W.; Ye, L.; Zhang, S.; Liu, S.; Ade, H.; Huang, F.; Hou, J. *Adv. Mater.* **2014**, *26*, 4043−4049.
(45) Wang, F.; Yu, H.; Xu, H.; Zhao, N. *Adv. Funct. Mater.* **2015**, DOI: 10.1002/adfm.201404007.
(46) Xiao, M.; Huang, F.; Huang, W.; Dkhissi, Y.; Zhu, Y.; Etheridgr, J.; Gray-Weale, A.; Bach, U.; Cheng, Y.-B.; Spiccia, L. *Angew. Chem., Int. Ed.* **2014**, *53*, 9898−9903.
(47) Chen, W.; Wu, H.; Liu, J.; Qin, C.; Yang, X.; Islam, A.; Cheng, Y.-B.; Han, L. *Energy Environ. Sci.* **2015**, *8*, 629−640.
(48) Ryu, S.; Seo, J.; Shin, S.; Kim, Y. C.; Jeon, N. J.; Noh, J. H.; Seok, S., II *J. Mater. Chem. A* **2015**, *3*, 3271−3275.
(49) Zhang, W.; Saliba, M.; Moore, D. T.; Pathak, S. K.; Horantner, M. T.; Stergiopoulos, T.; Stranks, S. D.; Eperon, G. E.; Alexander-Webber, J. A.; Abate, A.; et al. *Nat. Commun.* **2015**, *6*, 6142.
(50) Eperon, G.; Burlakov, V. M.; Docampo, P.; Goriely, A.; Snaith, H. J. *Adv. Funct. Mater.* **2014**, *24*, 151−157.
(51) Dualeh, A.; Tétreault, A.; Moehl, T.; Gao, P.; Nazeeruddin, M. K.; Grätzel, M. *Adv. Funct. Mater.* **2014**, *24*, 3250−3258.
(52) Kim, J. H.; Liang, P.-W.; Williams, S. T.; Cho, N.; Chueh, C.-C.; Glaz, M. S.; Ginger, D. S.; Jen, A. K.-Y. *Adv. Mater.* **2015**, *27*, 695−701.
(53) Zhou, H.; Zhang, Y.; Mai, C.-K.; Collins, S. D.; Nguyen, T.-Q.; Bazan, G. C.; Heeger, A. J. *Adv. Mater.* **2014**, *26*, 780−785.
(54) Tan, Z.; Zhang, W.; Zhang, Z.; Qian, D.; Huang, Y.; Hou, J.; Li, Y. *Adv. Mater.* **2012**, *24*, 1476−1481.
(55) Unger, E. L.; Hoke, E. t.; Bailie, C. D.; Nguyen, W. H.; Bowring, A. R.; Heumüller, T.; Christoforo, M. G.; McGehee, M. D. *Energy Environ. Sci.* **2014**, *7*, 3690−3698.
(56) Sanchez, R. S.; Gonzalez-Pedro, V.; Lee, J.-W.; Park, N.-G.; Kang, Y. S.; Mora-Sero, I.; Bisquert, J. *J. Phys. Chem. Lett.* **2014**, *5*, 2357−2363.
(57) Kim, H. S.; Park, N. G. *J. Phys. Chem. Lett.* **2014**, *5*, 2927−2934.

(58) Lee, M.; Teuscher, J.; Miyasaka, T.; Murakami, T. N.; Snaith, H. J. *Science* **2012**, *348*, 643−647.